Analytica Chimica Acta 1140 (2020) 145–152

Contents lists available at ScienceDirect

Analytica Chimica Acta

journal homepage: www.elsevier.com/locate/aca

A novel oriented immunosensor based on AuNPs-thionine-CMWCNTs and staphylococcal protein A for interleukin-6 analysis in complicated biological samples

Zihua Wang , Shengnan Yang , Yunyun Wang , Wei Feng , Binshuai Li , Jun Jiao , Bingkai Han , Qiang Chen *

The Key Laboratory of Bioactive Materials Ministry of Education, College of Life Science, Nankai University, Weijin Road No.94, Tianjin, 300071, PR China

HIGHLIGHTS

- The AuNPs-Thionine-CMWCNTs was synthesized in a simple way via co-valent linkage.
- SPA connects the Fc portion of the antibody to form oriented immunosensor.
- The linear range of the obtained sensor have involved in the IL-6 levels of AMI.
- The sensitive IL-6 immunosensor has been successfully applied in model rats.
- The biosensor exhibited great potential to evaluate the inflammatory response.

GRAPHICAL ABSTRACT

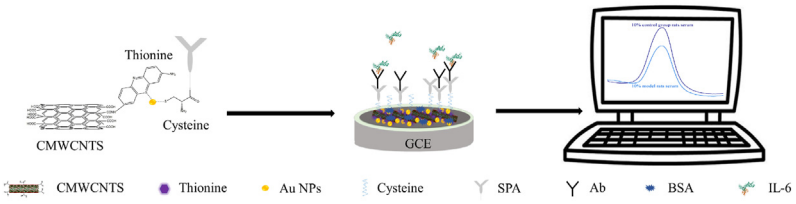

ARTICLE INFO

Article history:
Received 8 August 2020
Received in revised form
22 September 2020
Accepted 13 October 2020
Available online 16 October 2020

Keywords:
Staphylococcal protein A
Cysteine
Oriented immunosensor
Interleukin-6
Myocardial infarction

ABSTRACT

Interleukin-6 (IL-6) is of high importance for disease diagnosis and prognosis in human health since it's a crucial component in immune homeostasis, hematopoiesis, and metabolism. Herein, an immunosensor has been developed for monitoring IL-6, which is fabricated by Au nanoparticles (Au NPs)-thionine (THI)-carboxylated multi walled carbon nanotubes (CMWCNTs) as the substrate with high conductivity. Staphylococcal protein A (SPA) could directionally capture antibody to reduce steric hindrance caused by random immobilization. Built upon the high efficiency of IL-6 antibody immobilization by the SPA on the sensing surface, the immunosensor exhibited a favorable activity for IL-6 detection. Under optimal conditions, the biosensor presented a LOD of 2.87 pg mL^{-1} and a wide linear range from 0.01 ng mL^{-1} to 800 ng mL^{-1} in serum samples. Furthermore, the assembled sensor successfully quantified the IL-6 concentration in serum and different tissue lapping liquids (lung, heart, liver) from rats with myocardial infarction. The satisfactory performance of the proposed sensor not only broadens its application in clinical monitoring of IL-6 but also provides a novel approach to study inflammation in rats.

© 2020 Published by Elsevier B.V.

1. Introduction

Cardiovascular diseases (CVD), a chronic non-communicable disease, is a group of developmental disorders affecting the heart

* Corresponding author
E-mail address: qiangchen@nankai.edu.cn (Q. Chen).

https://doi.org/10.1016/j.aca.2020.10.025
0003-2670/© 2020 Published by Elsevier B.V.

and blood vessels with high incidence and mortality rate, including cardiac arrhythmia, myocardial ischemia, stroke, heart failure, acute myocardial infarction (AMI) and so on [1]. AMI is a life-threatening one in CVD, caused by partial or complete epicardial coronary artery occlusion as a result of plaque rupture or superficial erosion [2]. The existed plaques have evidence of stimulating the secretion of pro-inflammatory factors, which leads to inflammation erosion [3]. As a 185 amino acid polypeptide, interleukin-6 (IL-6) is a member of the multifunctional cytokine family with pro- and anti-inflammatory effects [4]. It is not only a factor that causing inflammation but also relative to the regulation of cardiac metabolism [5]. Diverse diseases like leukemia, Alzheimer's Disease, psoriasis, and sepsis also reveal an abnormal level of IL-6, thus making it become an important biomarker [6]. Therefore, in order to facilitate the intervention and management of diseases, there is a huge demand for the development of accurate methods for IL-6 monitoring. Additionally, quantification of IL-6 in rats will also benefit the assessments of inflammatory response aroused by the target drug contributing to the pharmacodynamic evaluation.

Although a series of methods for determining the IL-6 concentration have been developed, such as enzyme-linked immunosorbent assay (ELISA) [7], conductometric instrument [8], and organic electrochemical transistors [9], drawbacks like time-consuming procedures, sophisticated processes, and effortful pretreatment impede their further practical value. Currently, electrochemical sensors have gained extensive absorption in the field of medicine owing to its advantages of instant response, simplicity, and cost-effectiveness [10]. Electrochemical immunosensors have been widely explored to quantify IL-6 via immobilization of antibody [11–13], but the chaotic location of asymmetric macromolecules on supporting surfaces decreases their biological activities [14]. In addition, the IL-6 circulating in body fluids is in a tiny amount with nano and picomole scale [15]. Due to the level of IL-6 in AMI is 28.5–46.5 pg mL^{-1}, the immunosensor is meeting a challenge to attain a low enough detection limit and a wide linear range to further application in disease diagnosis [16].

To data, composing novel substrate materials with significant conductivity and biocompatibility and increasing the efficiency of antibody immobilization are the compelling strategies to improve the properties of the immunosensors [17]. Carbon-based materials, metallic nanoparticles, and electroactive substances have attracted considerable interest in the modification of sensing surface because of their distinguished electrochemical properties in enhancing conductivity and chemical stability [18]. Multi walled carbon nanotubes (MWCNTs) are well-known carbon nanomaterials with high conductivity, but the low solubility blocks their further applications [19]. Carboxylation of MWCNTs is an efficient way to solve such the problem, while CMWCNTs will also provide more binding sites due to the introduction of the carboxyl group [20,21]. Thionine (THI), as a cationic phenothiazine accelerating electron transfer, is a remarkable electroactive substance attributing to its exceptional ability on fastening electron transfer, electrochemical reversibility, and stability [22]. The CMWCNTs will strongly bind to THI through π–π interaction, electrostatic interaction, and amide bonds, which benefit the sensitivity and long-term stability of the sensor [23,24]. Besides, thionine also has the capacity as a linker to further anchor Au nanoparticles on the supporting materials via the mercapto group. Gold nanoparticles are outstanding candidates for immobilization of biological protein to detect biological events, exhibiting an active specific surface area with great capacity, negligible toxicity, and high affinity to bonding biomolecules, which makes the biosensor biocompatible and sensitive [25,26].

Apart from the enhanced conductivity, the more effective antibody is fixed, the better sensing performance will be obtained. Firstly, directional immobilization of antibody is a key to improving sensitivity and stability. Staphylococcal protein A (SPA), as a cytoderm unit of staphylococcus aureus, connects the Fc portion of the antibody directionally and leaves the Fab portion to catch the antigen, which improves the binding capacity towards target analyte and reduces the loss of biological activity due to the decrease on steric hindrance [14,27,28]. On the other hand, the appropriate connecting approaches between biomolecules like SPA and the sensing surface, including ionic interactions, hydrophobic interactions, dative binding, bifunctional linkers or mediator linkers, and chemisorption via thiol derivatives, also have impacts on the effectiveness of antibody immobilization [29]. Bifunctional linkers are increasingly utilized in the connecting biological compounds owing to their specific binding sites, which will finally enhance the specificity and stability of the sensor [30]. As a bifunctional linker involving multifunctional groups, cysteine (Cys) will make AuNPs covalently connect protein, effectively improving the ability of detection via forming a stable complex [31–34]. Thus, SPA-Cys-AuNPs-THI-CMWCNTs could be a sensing platform to accomplish precisely and speedily electrochemical recognition of IL-6.

Herein, an ultrasensitive immunosensor has been proposed based on Ab-SPA-Cys-AuNPs-THI-CMWCNTs nanocomposites for IL-6 detection. First of all, THI-CMWCNTs were synthesized through π–π stacking and amide bonds. After loading with AuNPs by thionine as the linker, AuNPs -THI-CMWCNTs nanohybrids were functionalized with SPA via cysteine. With orientated immobilization of IL-6 antibody, the electrochemical immunosensor has been successfully fabricated based on the antigen-antibody coupling event. The decline in random orientation and steric-hindrance guaranteed the obtained sensor owning a satisfactory specificity. Moreover, the impacts of AuNPs size on the analytic perfoemance of the sensor also has been investigated in this work. There was a remarkable linear relationship between the current response and the concentration of IL-6, and the sensor earned a LOD of 2.87 pg mL^{-1} with a wide linear range from 0.01 ng mL^{-1} to 800 ng mL^{-1} in serum samples. With the presence or absence of drugs, the proposed immunosensor successfully accomplished the detection of IL-6 in myocardial infarction rats. The proposed immunosensor can be an ideal platform for detecting trace IL-6 in a complex matrix, facilitating further study on AMI and investigation of the inflammatory response in drug discovery.

2. Experimental

2.1. Reagents and materials

Sodium dihydrogen phosphate ($NaH_2PO_4 \cdot 2H_2O$), Gold (III) chloride trihydrate, dibasic sodium phosphate ($Na_2HPO_4 \cdot 12H_2O$), *N*-(3-dimethylaminopropyl)-*N′*-ethylcarbodiimide hydrochloride (EDC), *N*-hydroxysuccinimide (NHS), Cysteamine (Cys), potassium chloride (KCl), potassium ferricyanide ($K_3Fe[(CN)_6]$), Albumin from bovine serum (BSA), Glucose Oxidase (GOD), Cholesterol esterase (ChOx), Salvianic acid A sodium (SAA) were all purchased from Sigma-Aldrich Inc. (St. Louis, MO, USA). Thionine chloride was purchased form Solarbio Inc. L-Ascorbic acid (AA) was purchased from VETEC Inc. MWCNTs (30–50 nm) was purchased from the Institute of Organic Chemistry, Chinese Academy of Sciences (Chengdu, China). Staphylococcal protein A (SPA, MW:46,742) was purchased from Thermo Scientific Inc. Rats IL-6 Enzyme Linked Immunosorbent Assay Kit, IL-6, IL-6 Antibody, interleukin-1 (IL-1), interleukin-10 (IL-10), and insulin were purchased from R&D system. CA125 was purchased from Abnova. Alpha-fetoprotein (AFP) was purchased from Biorbyt (European). Isoproterenol Hydrochloride (ISO), Chloral Hydrate were purchased from TCI Shanghai. Radioimmunoprecipitation assay (RIPA) was purchased from New Cell and Molecular Biotech Co. The chemicals were used without treatment, and ultrapure water was used throughout all experiments.

2.2. Synthesis of AuNPs-THI-CMWCNTs nanomaterials

CMWCNTs were synthesized based on our previous report [35]. CMWCNTs was ultrasonically dissolved in 20 mL water for 90 min and supplied 2 mM EDC and 2 mM NHS. After adding 20 mL THI solution (1 mg mL^{-1}), the reaction was kept for 6 h under vigorous stirring. The amino groups of THI and terminal carboxyl groups of CMWCNTs were covalently bound via the formation of amide bonds. Then 20 mM 2-mercaptoethanol was added into the mixture. The THI-CMWCNTs was resuspended in ddH_2O, followed by centrifugation with 8000 rpm to remove the excess agents. For synthesis of AuNPs-THI-CMWCNTs, 10 mM $HAuCl_4$ and 0.1 M AA were injected into the above mixture and stirred under room temperature for 2 h. Finally, the product was collected by centrifugation and washed by ddH_2O for three times. After overnight dried in the vacuum drying oven, the AuNPs-THI-CMWCNTs nanomaterials were stored at 4 °C refrigerator. The methods of different sizes of AuNPs were shown in supplementary material.

2.3. Fabrication of the proposed IL-6 immunosensor

The prepared process of IL-6 biosensor was presented in Scheme 1. The glass carbon electrode (3 mm, GCE) was furbished by alumina powder (0.1 and 0.05 μm) before modification, followed by washing with water and absolute ethanol for 3 min, respectively, and then dried under nitrogen gas. The 8 μL AuNPs-THI-CMWCNTs suspension was drop coated onto a purified GCE and desiccated in air under room temperature to obtain AuNPs-THI-CMWCNTs/GCE. Due to cysteine (Cys) contains carboxyl, amino and sulfhydryl groups, AuNPs-THI-CMWCNTs/GCE was immersed in 5 mM Cys solution to form carboxyl/amino group surface by Au—S. Whereafter, 2 mM EDC and 5 mM NHS were dropped onto the electrode for 15 min, and then the surface was incubated with 2 mg mL^{-1} SPA solution at 4 °C. After the modified electrode immersed in 1.5 mg mL^{-1} Ab, the Fc fragment of Ab selectively binds with SPA to form oriented immobilization immunosensor. The 1% BSA was used to debride non-specific binding sites and blocked the surface of electrode. Subsequently, the assembled sensor was bathed with different concentration of IL-6 for testing. In each modification process, the proposed electrode was washed stepwise with the PBS buffer solution (100 mM, pH 7.4) to remove unconnected molecules on the electrode surface and stored at 4 °C for later research.

2.4. Apparatus and electrochemical methods

Transmission electron microscopy (TEM), energy-dispersive X-ray spectroscopy (EDX) images and mapping images were obtained using Philips Tecnai G2 F20 instrument (Amsterdam, Holland). Fourier transform infrared spectroscopy (FTIR) measurements and X-ray diffraction (XRD) measurements were collected with a Bruker TENSOR 37 (Karlsruhe, Germany) and Rigaku D/max-rA with Cu Kα radiation (Rigaku, Japan). CHI 760 E electrochemical workstation (Shanghai CH Instrument with 760 E software, China) was used for the electrochemical experiments. An ordinary three-electrode system was used as electrochemical system, including working electrode (modified GCE), counter electrode (1 mm Pt wire), reference electrode (Ag/AgCl electrode with potassium chloride supersaturated solution). All the electrochemical tests were carried out under ambient temperature in 5 mM 40 mL $[Fe(CN)_6]^{3-/4-}$ aqueous solution with 0.1 M KCl.

2.5. Preparation of practical samples and rat model

Conforming to the Chinese Medical Ethics Committee ground rules of animal experiments and ARRIVE, all procedures were conducted with ethical principles for animal research. Before the experiment, the animals were fed with half of the light/dark day, and free access to commercial standard rat cube diet and water at 25 °C for 7 days.

Sprague—Dawley male rats (190~210 g, SPF grade, NO.1112512011000006) were purchased from the National Institutes for Food and Drug Control (Daxing). ISO increases heart rate and triggers cardiac hypertrophy and ultimately myocardial infarction and injury [36], which employed make for model rats of myocardial infarction. Rats were aimlessly classified into 4 groups (each group 6 rats): (1) normal control group (Con), received equivalent physiological saline (i.p.) for 11 days; (2) ISO_{20} group, received normal saline (i.p.) for 7 days and ISO injection daily (20 mg/kg, i. p., dissolved in physiological saline) for 4 days; (3) ISO_{80} group, same as ISO_{20} group, but the concentration of ISO was 80 mg/kg; (4) SAA + ISO_{80} group, daily received SAA (3 mg/kg, i. g.) for 7 days and ISO injection (80 mg/kg, i. p.) for last 4 days. Rats were starved overnight before the end of the experiment, and anesthetized with 10% chloral hydrate (i.p.). The heart, liver, and lung tissue (1 mg) were disrupted with the grinding tube in RIPA (10 mL) lysis buffer, then the tissues were incubated for 30 min on ice. With centrifugation at 3000 rpm for 10 min at 4 °C, the

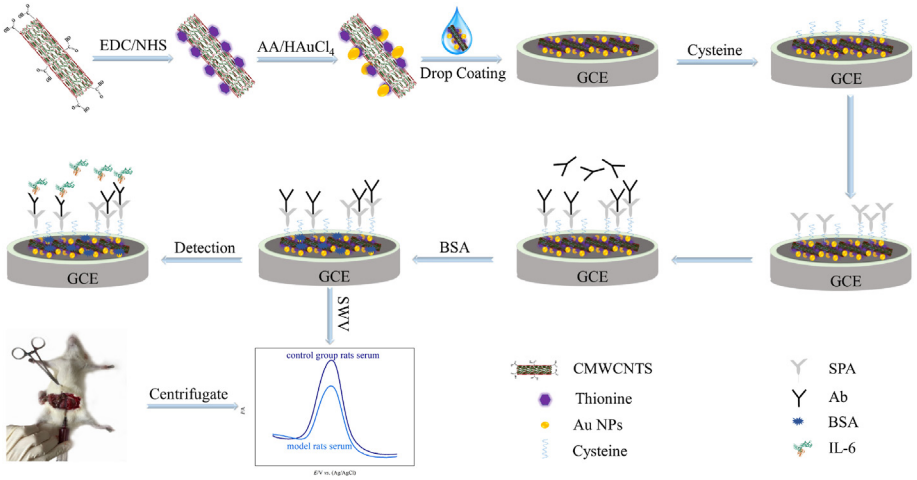

Scheme 1. The preparation procedure of IL-6 immunosensor working electrode.

epipelagic solution was gained. The blood was collected from the operation with the abdominal aorta and incubated at room temperature until blood clotted. After centrifugation at 2000 rpm for 5 min at 4 °C, the lymph was collected and deposited at −80 °C for further assessment. The serum and supernatants were diluted to 10% before the electrochemical experiments.

3. Results and discussion

3.1. Structure presentation

To verify the microstructure and morphological features of AuNPs-THI-CMWCNTs nanocomposites, the complex was identified by TEM. As shown in Fig. 1A, CMWCNTs exhibited an open terminal with defects indicating the pristine MWCNTS were successfully oxidized, which resulted in an improved solubility in water. Fig. 1B displays the TEM image of AuNPs-THI-CMWCNTs. Apparently, THI-CMWCNTs maintained their original tubular structures, implying that the addition of thionine did not change the morphology of CMWCNTs. Meanwhile, AuNPs (around 18.49 nm in diameter) were also well loaded on the surface of THI-CMWCNTs, which may result from the formation of Au—N bond and Au—S bond between AuNPs and THI [37]. As shown in the EDX spectrum in Fig. S1, the occurrence of C, O, S and Au elements could further testify that gold nanoparticles had been introduced on the surface of THI-CMWCNTs. Element mapping was conducted to confirm the element distribution (Fig. 1C). It can be clearly seen that the C, O and S elements were full of the view, while Au and S element obviously blended together, revealing that AuNPs could be anchored onto the nanocomposites on account of the special structure of THI.

FT-IR and XRD were employed to confirm the combinational properties and crystallinity of the AuNPs-THI-CMWCNTs nanocomposites in Fig. 1D and E. As displayed in Fig. 1D, the band at 1630 cm^{-1},1600 cm^{-1} and 1500 cm^{-1} due to the stretching frequencies of C=O and the aromatic ring of THI [38], respectively. The weak absorption band at 901 cm^{-1} was divided to C—S, while 1650-1390 cm^{-1} was attributed to Amide II, indicating a covalent linkage between THI and CMWCNTs [39]. The secondary amine of the THI stretching in AuNPs-THI-CMWCNTs emerged at 1625 cm^{-1}, suggesting that AuNPs favorably bound to THI-CMWCNTs surfaces [40]. The XRD spectra of the MWCNTs, CMWCNTs, THI-CMWCNTs and AuNPs-THI-CMWCNTs are shown in Fig. 1E. MWCNTs presented characteristic peaks around 25.98°, whereas smooth peaks appeared after the formation of CMWCNTs, which confirmed the MWCNTs had been oxidized successfully. The 2θ values of 38.2°, 44.42°, 64.6°, 77.64° and 81.74°, which can be assigned to the (111), (200), (220), (311) and (222) reflections of AuNPs [41], respectively. All the results reveal that the Au-THI-CMWCNTs nanocomposites had been successfully synthesized.

3.2. Electrochemical characterization

The electron transfer of the proposed electrodes was determined in a KCl (100 mM) aqueous solution by cyclic voltammograms using the ferro/ferricyanide redox system as a probe. In Fig. 3A, the modified GCE exhibited a pair of chiseled redox peak of $Fe^{2+/3+}$ at around 290/165 mV and the peak-to-peak separation (ΔEp) was half of bare GCE. The active surface area of all the above sensors was computed from the Randles—Sevcik equation [42]:

$$i_p = 2.69 \times 10^5 n^{3/2} D^{1/2} C_0 \nu^{1/2} A_{eff} \quad [1]$$

where i_p represents the redox peak current (μA), n is the number of transferred electrons, D is relate to the diffusion coefficient of ferricyanide solution (6.70 ± 0.02) × 10^{-6} cm^2 s^{-1}), C_0 is the concentration of the probe molecule (10 mM), ν is the scan rate (100 mV s^{-1}), and A_{eff} is effective surface area of the electrode (cm^2) can be calculated by the equation. AuNPs-THI-CMWCNTs/GCE (curve d) gained the largest electroactive surface area, and 1.13, 1.32, 2.14 times higher than THI-CMWCNTs/GCE (curve c), CMWCNTs/GCE (curve b) and GCE (curve a). This phenomenon can be explained by the following reasons: (1) CMWCNTs with more open ends and defects not only offer a better charge transfer to enhance the electrical conductivity of nanomaterials, but also enlarge the active surface area providing more binding sites. (2) THI, as an electroactive substance, aids the redox of $Fe^{2+/3+}$ and acceleration of electron transfer through amide bonds and π—π stacking interaction with CMWCNTs. (3) The phenothiazinium moiety of THI makes it as a linker to fix AuNPs on the surface of CMWCNTs without complicated procedures. (4) AuNPs efficiently enhance the effective surface area of the GCE, which improves the conductivity and enables to immobilized biomolecules on the sensing electrode by bioconjugation. Therefore, the AuNPs-THI-CMWCNTs nanocomposites with significantly electrochemical properties can be a suitable supporting matrix for improving performances of the immunosensor.

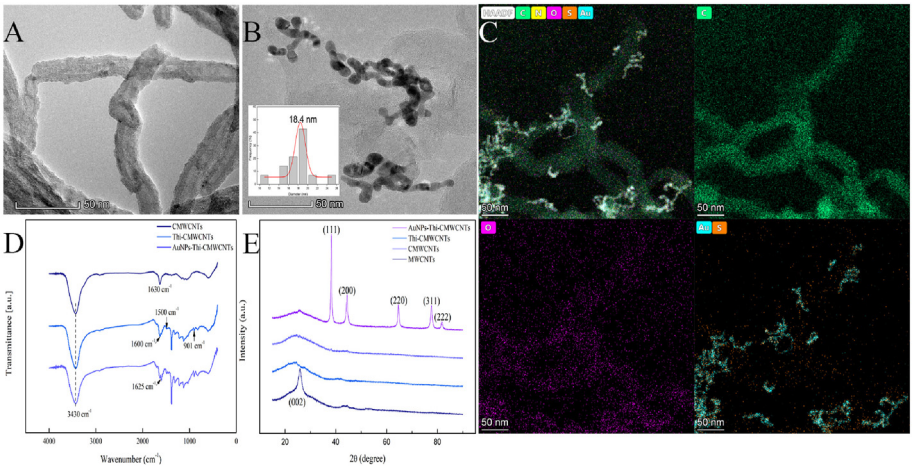

Fig. 1. TEM images of (A) CMWCNTs and (B) AuNPs-THI-CMWCNTs and insert shows the distribution of diameter for this sample (C) Elemental mapping images of AuNPs-THI-CMWCNTs. (D) FTIR and (E) XRD images of different modifications.

The electrochemical behavior of the stepwise decorated immunosensor were researched and shown in Fig. 2B. When SPA (curve b), BSA (curve c), and IL-6 Ab (curve d) were immobilized layer by layer on Cys-AuNPs-THI-CMWCNTs/GCE, compared to the pristine one (curve a), the current peaks decreased 0.91, 0.85, and 0.71 times, respectively, since the modified non-conductive protein molecules hampered the electron transfer. It also proved the immunosensor was assembled successfully. In addition, along with the increasing concentration of IL-6, a further decline could be observed in the peak current (curve e and f) by the electrochemical measurement on Ab-BSA-SPA-Cys-AuNPs-THI-CMWCNTs/GCE. This slight current change gave the as-prepared GCE an opportunity to be a potential platform for monitoring IL-6 levels. Electrochemical impedance spectroscopy (EIS) displayed the step-by-step decorating process of the sensor. As shown in Fig. 2C, with the stepwise decoration on the electrode surface, resistance (Rct) remarkably decreased implying that the nanomaterials accelerated the electron transfer. As shown in Fig. 2D, when SPA, Ab, BSA, IL-6 modified the AuNPs-THI-CMWCNTs, the Rct values were increased constantly, owing to the insulation of biomaterials. The results of EIS were consistent with all the electrochemical behaviors in Fig. 2A and B, demonstrating the IL-6 biosensor was formed successfully.

3.3. Optimization conditions of the fabricated immunosensor

To compare the effects of AuNPs size, the analytical abilities of the obtained nanomaterials also had been investigated in this work. As shown in Fig. S2, AuNPs with different size of 5.5 nm, and 42.1 nm were synthesized successfully. The smaller AuNPs revealed higher conductivities than their counterparts (Fig. S2C). However, it can be clearly seen in Fig. S3A that the larger nanoparticles displayed more enhancements on the ΔI since the smaller ones have strong coulomb repulsion which are not conducive to protein immobilization [43]. Due to the surface of gold nanoparticles is always deficient in electron, the affinity to electrons will reduce

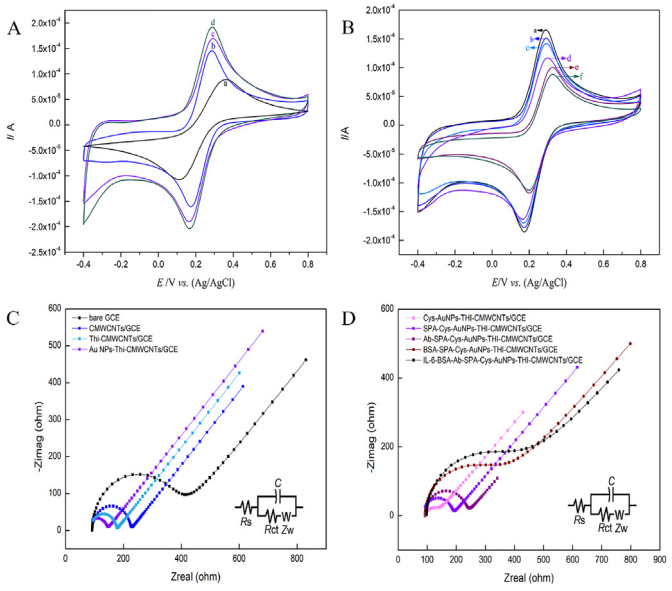

Fig. 2. (A) CV curves of (a) GCE, (b) CMWCNTs/GCE, (c) THI-CMWCNTs/GCE, (d) AuNPs-THI-CMWCNTs/GCE; (B) CV curves of (a) Cys-AuNPs-THI-CMWCNTs/GCE, (b) SPA-Cys-AuNPs-THI-CMWCNTs/GCE, (c) BSA-SPA-Cys-AuNPs-THI-CMWCNTs/GCE, (d) Ab-BSA-SPA-Cys-AuNPs-THI-CMWCNTs/GCE, (e) IL-6 (10 ng)-BSA-Ab-SPA-Cys-AuNPs-THI-CMWCNTs/GCE, (f) IL-6 (80 ng)-BSA-Ab-SPA-Cys-AuNPs-THI-CMWCNTs/GCE in 5 mM $[Fe(CN)_6]^{3-/4-}$ solution (containing 100 mM KCl). EIS (C and D) of the step-modified immunosensors and the inset shows the equivalent circuit.

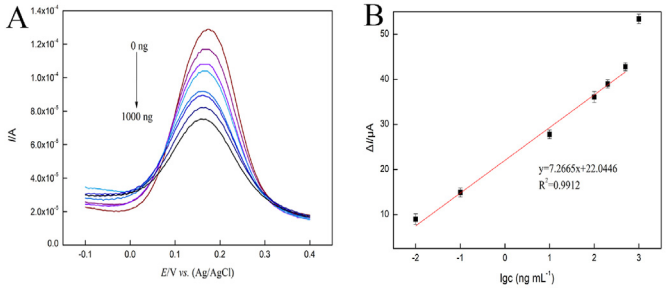

Fig. 3. (A) SWV of the immunosensor for the determination of different concentrations of IL-6 from 0 ng mL^{-1} to 1000 ng mL^{-1} (0.01, 0.1, 10, 100, 200, 800 and 1000 ng mL^{-1}). (B) Calibration curves of the immunosensor to different concentrations of IL-6. Error bar = RSD (n = 5).

with the increase of dimension, thus the nanohybrids based on over 18.4 nm exhibiting a weaken electrochemical property. Therefore, 18.4 nm AuNPs were chosen for further experiments.

The immobilization conditions including the incubation time, pH and temperature were optimized in accordance with the best sensing response (Fig. S3). Firstly, the SPA incubation time in the formation of the immunocomplex impacts on the performance of the designed sensor. In Fig. S3B, the ΔI ($\Delta I = I_{peak_0} - I_{peak_i}$, I_{peak_0} is the peak current with 0 ng IL-6 in $[Fe(CN)_6]^{3-/4-}$) increased obviously when the incubation time extended from 40 min to 60 min. However, a longer incubation time over 60 min did not heighten the ΔI significantly. As a result, 60 min was selected for linking SPA in the assembling process. For the incubation time of IL-6 antibody (Fig. S3C), the response current distinctly boosted until 25min. When the incubation continued, the ΔI tended to smooth with a slightly decrease, indicating the optimal time for IL-6 antibody was 25 min. The same phenomenon can be observed when incubated with IL-6 in Fig. S3D because the proper concentration fortified specific binding between Ab and IL-6, but the excessive thickness film hindered electron transfer. As a result, 25 min was chosen for IL-6 in further detection.

With different pH values, the PBS aqueous solution greatly influenced the behavior of proposed sensor because the excessive acidity and alkalinity could impair the activity of bioactive substances and the linkage of antigen-antibody. As shown in Fig. S3E, the best ΔI was obtained in pH 7.5 PBS solution. The sensitivity of the immunosensor relied on the test temperature, thus the IL-6 immunosensor was experimentally performed at a temperature range of 5–45 °C. The ΔI grew with the temperature risen from 5 °C to 35 °C, and then decreased with the variation of temperature from 35 °C to 45 °C, which indicated that suitable increase of temperature facilitated the combination of Ab and IL-6, and excessive temperature destroyed the chemical structure of the bioactive materials. Hence, pH 7.5 and 35 °C were selected for the follow-up research.

3.4. Quantitative capability of the IL-6 immunosensor

With comparatively high sensitivity and less time, square wave voltammetry (SWV) has been a powerful technique in analytical measurement. Therefore, SWV was utilized to verify the analytic ability of the established label-free sensor towards different levels of IL-6 and shown in Fig. 3A. With the IL-6 concentrations increasing from 0 ng mL^{-1} to 1000 ng mL^{-1}, the ΔI values have decreased accordingly under the selected experimental conditions. By calculation, the semi-log plot of ΔI and IL-6 concentration showed a strong linear relationship in the range from 0.01 ng mL^{-1} to 800 ng mL^{-1}. After fitting the relationship between the lgC and

the ΔI, the equation of linear regression was $\Delta I = 7.2665\lg C + 22.0446$, with a correlation coefficient of 0.9912. From Fig. 3B (the calibration plot), the detection limit of about 2.87 pg mL^{-1} (S/N = 3). Compared with the recorded IL-6 method and sensor tabulated in Table 1, the proposed immunosensor showed an outstanding sensitivity and distinguished application in serum samples and tissue lapping fluid.

3.5. Specificity, stability, reproducibility and applicability of the IL-6 immunosensor

Specificity is a crucial parameter for an immunosensor, which ensures it can discriminate the target analyst among complicated substrates or biological samples without further separation and extraction. The specificity and nonspecific absorption of the presented IL-6 immunosensor have been assessed in blank serum and serum with seven interferences, namely IL-1, IL-10, insulin, CA125, AFP, ChOx, and GOD. The current changes were recorded by SWV and depicted in Fig. 4A. The peak currents caused by interfering substances and blank serum were relatively weak, suggesting that the nonspecific absorptions were rare on the proposed sensing surface. In contrast to the single, the ΔI of IL-6 (30 ng mL^{-1}) with seven proteins changed less than 4.5% implying that the current responses on the prepared sensor could not be affected by these interferences. The above results revealed that the proposed Ab-SPA-Cys-AuNPs-THI-CMWCNTs/GCE was highly specific and selective for detection of IL-6 under the physiological conditions.

Besides, the reproducibility is also a considerable indicator to figure out the accuracy of the obtained sensor. It was investigated by parallel SWV measurements using five independent Ab-SPA-Cys-AuNPs-THI-CMWCNTs modified electrodes (Fig. 4B). The relative stand deviation (RSD) of the prepared biosensor was 2.45%, demonstrating a good reproducibility of the proposed immunosensor. As longstanding stability, the immunosensor was assessed by testing the ΔI on five working electrodes at an interval of 5 days. The unused proposed immunosensors were stored at 4 °C with pH 7.4 PBS buffer in the refrigerator. As seen in Fig. 4C, the ΔI remained 90.8% of the original current response after 30 days. Therefore, the above results reveal that Ab-SPA-Cys-AuNPs-THI-CMWCNTs nanohybrids can serve as an admirable electrode modifier for the quantification of IL-6 with satisfactory properties in specificity, reproductivity, and stability.

The pragmatic feasibility and applicability of the prepared sensor were assessed for detection of IL-6 in the real sample. As shown in Table S1, IL-6 were carried out by both the proposed sensor and commercial ELISA kits in 10% diluted human serum samples for recovery experiments. With 15, 20 and 30 ng mL^{-1} IL-6 added in human diluted serum samples, the RSD of immunosensor was in the range from 2.05% to 3.22% with the recovery rate of immunosensor from 98.3% to 101.4% between two methods. The results demonstrated that the proposed immunosensor had an acceptable feasibility for analysis of IL-6 in serum samples.

3.6. Detection of IL-6 released from animal model

As a β-adrenoceptor agonist, ISO can cause a contractile dysfunction of the left ventricle, with increasing end-diastolic volume and end-diastolic pressure leading to the cardiac remodeling [47]. Rats with ISO-induced myocardial infarction can serve as a typical model to study myocardial infarction in human since the pathophysiological and morphologic alterations in noncoronary myocardial necrotic rats are consistent with the lesions in human [48,49]. SAA is beneficial for the treatment of cardio- and cerebrovascular diseases, it is a water-soluble active component of natural medicine salvia miltiorrhiza. Evaluation of inflammatory response by IL-6 is one of the ways to assess the positive influence of SAA on myocardial infarction [50]. As shown in Fig. 5A, the IL-6 concentration increased with the increments of ISO, suggesting an inflammatory reaction has been risen by ISO in rat while the myocardial infarction had been set up successfully to some extent. Based on the ΔI, IL-6 concentration for ISO_{20}, ISO_{80}, and SAA + ISO_{80} were calculated to be 0.25, 0.43, and 0.35 ng mL^{-1} by the calibration equation in Fig. 3B. It can be seen that the concentration of IL-6 in SAA + ISO_{80} was obviously lower than its ISO_{80} counterpart, implying that SAA had protective effects for rats, consistent with the results reported by Song [51].

The inflammatory reactions in different tissues also had been explored by the immunosensor and ELISA kit in rats. As shown in Fig. 5B, after adding 100 pg mL^{-1} standard concentration of IL-6 in rat heart samples, two approaches both achieved the detection of IL-6 changes, indicating the proposed sensor has prominent practicality. In addition, the immunosensor had also been applied in the determination of IL-6 in the liver and lung tissue (Fig. 5C). Under the stimulation of ISO_{80}, liver tissue did not reveal a significant increase of IL-6 level. On the contrast, the inflammatory factor IL-6 had been obviously active in the lung ($P < 0.05$), consistent with the results of the ELISA kit ($P < 0.01$), further confirming the reliability of the obtained immunosensor in the animal model. Therefore, IL-6 immunosensor has the capacity of evaluating inflammatory response in the animal model, providing an attractive approach for the in-depth study on inflammatory response during drug discovery.

4. Conclusions

In general, we established a fast orientation immunosensor based on Ab-SPA-Cys-AuNPs-THI-CMWCNTs/GCE. It earned a strong linear relationship between ΔI and IL-6 concentration with a

Table 1
The different methods for the detection of IL-6.

Measurement protocol	Signal strategies	Linear range (ng/mL)	Detection limit (pg/mL)	Real samples	Reference
ELISA	*anti*-IL6	0.039–2.5	39	human serum samples	[7]
conductometric immunosensor	HRP-*anti*-IL6-modified nanogold	0.025–0.4	5	human serum samples	[8]
colorimetric sensor	Au@Ag bimetallic nanoparticles	0.011–1.8	11	human serum samples	[44]
electrochemical transistors	Au-EG_6COOH electrodes	0.22–2.2	220	glycine–HCl buffer	[45]
electrochemical transistors	aptameric graphene-based field effect transistor	0.02–0.8	12.2	saliva	[9]
electrochemical immunosensor	Gold micro disc electrodes	0.02–0.06	20	serum samples	[46]
electrochemical immunosensor	Ab-SPA-Cys-Au NPs- THI -CMWCNTs/GCE	0.01–800	2.87	serum samples, model rat serum and tissue lapping fluid	This work

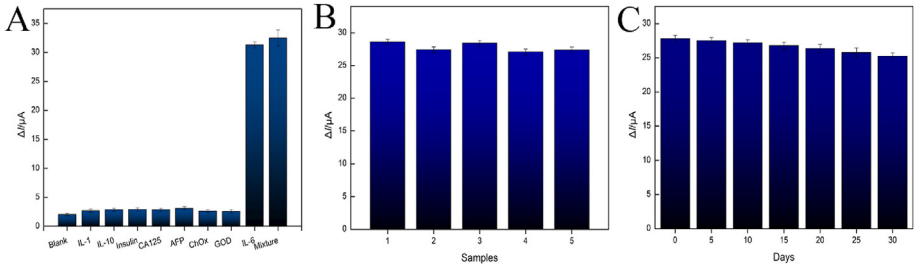

Fig. 4. (A) The specificity of the Ab-SPA-Cys-AuNPs-THI-CMWCNTs immunosensor for the 100 ng mL^{-1} other proteins and 30 ng mL^{-1} IL-6. (B) The ΔI of the 10 ng mL^{-1} IL-6 to different electrodes treated in same way. (C) The stability studies of the IL-6 immunosensor. Error bar = RSD (n = 5).

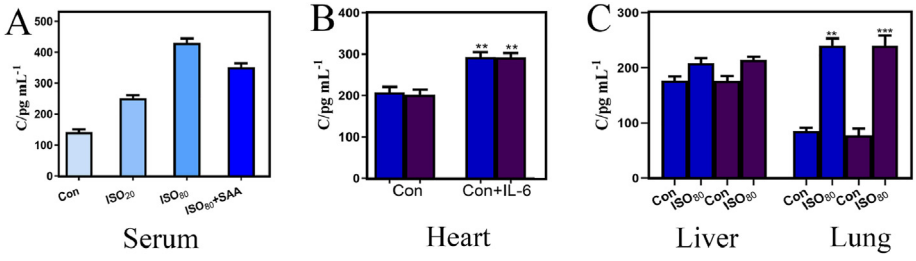

Fig. 5. (A) The IL-6 concentrations of Con, ISO_{20}, ISO_{80} and SAA + ISO_{80} in serum. (B) The IL-6 concentrations of control group and control group added 100 pg mL^{-1}, **P < 0.05 vs Con (n = 6). (C) The IL-6 concentrations of control group and ISO_{80}, **P < 0.05 vs Lung Con and ***P < 0.01 vs Lung Con (n = 6). (Blue column stands for immunosensor, Purple ones for ELISA). (For interpretation of the references to color in this figure legend, the reader is referred to the Web version of this article.)

detection limit of 2.87 pg mL^{-1}. By taking advantages of the remarkable specificity, stability, reproducibility, and applicability, we have successfully applied the prepared sensor for the quantitative measure of IL-6 in the animal model with admirable feasibility. Compared with ELISA, the proposed immunosensor has successfully captured the inflammatory response of cardiomyocytes in ISO-induced rats, with highly consistent results. Meanwhile, the immunosensor has the ability to analyze IL-6 differences among various tissues in the presence or absence of drugs, revealing an outstanding potential in pharmacodynamic evaluation. Thus, the present work not only provides a precise platform for quantification of IL-6 levels but also facilitates in-depth researches on inflammation-linked diseases and relative drug discovery in the prospect.

Funding

This work was supported by the National Natural Science Foundation of China [Grant Number: 81671779 and 81871451].

CRediT authorship contribution statement

Zihua Wang: Conceptualization, Methodology, Investigation, Formal analysis, Writing - original draft, Visualization, Writing - review & editing. **Shengnan Yang:** Investigation, Formal analysis. **Yunyun Wang:** Investigation, Validation. **Wei Feng:** Investigation. **Binshuai Li:** Writing - review & editing. **Jun Jiao:** Writing - review & editing. **Bingkai Han:** Writing - review & editing. **Qiang Chen:** Supervision, Project administration, Funding acquisition, Writing - review & editing.

Declaration of competing interest

The authors declare that they have no known competing financial interests or personal relationships that could have appeared to influence the work reported in this paper.

Appendix A. Supplementary data

Supplementary data to this article can be found online at https://doi.org/10.1016/j.aca.2020.10.025.

References

[1] Godugu Chandraiah, Kumari Preeti, Khurana Amit, Nanoyttria attenuates isoproterenol-induced cardiac injury, Nanomedicine 13 (23) (2018) 2961–2980.
[2] H.D. White, D.P. Chew, Acute myocardial infarction, Lancet 372 (9638) (2008) 570–584.
[3] D.R. Anderson, J.T. Poterucha, T.R. Mikuls, M.J. Duryee, R.P. Garvin, L.W. Klassen, S.W. Shurmur, G.M. Thiele, IL-6 and its receptors in coronary artery disease and acute myocardial infarction, Cytokine 62 (3) (2013) 395–400.
[4] J. Wolf, S. Rose-John, C. Garbers, Interleukin-6 and its receptors: a highly regulated and dynamic system, Cytokine 70 (1) (2014) 11–20.
[5] T. Kanda, T. Takahashi, <b>Interleukin-6 and cardiovascular diseases, Jpn. Heart J. 45 (2) (2004) 183–193.
[6] M.A. Khan, M. Mujahid, Recent advances in electrochemical and optical biosensors designed for detection of interleukin 6, Sensors 20 (3) (2020) 646.
[7] C.K. Turner, T.M. Blieden, T.J. Smith, S.E. Feldon, D.C. Foster, P.J. Sime, R.P. Phipps, A novel ELISpot method for adherent cells, J. Immunol. Methods 291 (1) (2004) 63–70.
[8] K.-Z. Liang, J.-S. Qi, W.-J. Mu, Z.-X. Liu, Conductometric immunoassay for interleukin-6 in human serum based on organic/inorganic hybrid membrane-functionalized interface, Bioproc. Biosyst. Eng. 32 (3) (2009) 353–359.
[9] Z. Hao, Y. Pan, W. Shao, Q. Lin, X. Zhao, Graphene-based fully integrated portable nanosensing system for on-line detection of cytokine biomarkers in saliva, Biosens. Bioelectron. 134 (2019) 16–23.
[10] Y. Boonyasit, O. Chailapakul, W. Laiwattanapaisal, A folding affinity paper-based electrochemical impedance device for cardiovascular risk assessment, Biosens. Bioelectron. 130 (2019) 389–396.
[11] Wenshu Zheng, Yiping Chen, Wenbo Yu, Binfeng Yin, Sang Joo, An enzyme-mediated competitive colorimetric sensor based on Au@Ag bimetallic nanoparticles for highly sensitive detection of disease biomarkers, Analyst: The Analytical Journal of the 142 (2017) 2954–2960. Royal Society of Chemistry: A Monthly International Publication Dealing with All Branches of Analytical Chemistry.
[12] J. Liu, M.A.A. Abdullah, L. Yang, J. Wang, Fast affinity induced reaction sensor based on a fluorogenic click reaction for quick detection of protein biomarkers, Anal. Chem. 92 (1) (2020) 647–653.
[13] G. Wang, X. He, L. Chen, Y. Zhu, X. Zhang, Ultrasensitive IL-6 electrochemical immunosensor based on Au nanoparticles-graphene-silica biointerface, Colloids Surf. B Biointerfaces 116 (2014) 714–719.

[14] B. Lu, M.R. Smyth, R. O'Kennedy, Tutorial review. Oriented immobilization of antibodies and its applications in immunoassays and immunosensors, Analyst 121 (1996).
[15] A. Kamińska, K. Winkler, A. Kowalska, E. Witkowska, T. Szymborski, A. Janeczek, J. Waluk, SERS-based immunoassay in a microfluidic system for the multiplexed recognition of interleukins from blood plasma: towards picogram detection, Sci. Rep. 7 (1) (2017) 10656.
[16] Y. Miyao, H. Yasue, H. Ogawa, I. Misumi, T. Masuda, T. Sakamoto, E. Morita, Elevated plasma interleukin-6 levels in patients with acute myocardial infarction, Am. Heart J. 126 (6) (1993) 1299–1304.
[17] H.-P. Peng, Y. Hu, A.-L. Liu, W. Chen, X.-H. Lin, X.-B. Yu, Label-free electrochemical immunosensor based on multi-functional gold nanoparticles–polydopamine–thionine–graphene oxide nanocomposites film for determination of alpha-fetoprotein, J. Electroanal. Chem. 712 (2014) 89–95.
[18] O.C. Compton, S.T. Nguyen, Graphene oxide, highly reduced graphene oxide, and graphene: versatile building blocks for carbon-based materials, Small 6 (6) (2010) 711–723.
[19] M. Bahgat, A.A. Farghali, W.M.A. El Rouby, M.H. Khedr, Synthesis and modification of multi-walled carbon nano-tubes (MWCNTs) for water treatment applications, J. Anal. Appl. Pyrol. 92 (2) (2011) 307–313.
[20] T.G. Ros, A.J. van Dillen, J.W. Geus, D.C. Koningsberger, Surface oxidation of carbon nanofibres, Chem. Eur J. 8 (5) (2002) 1151–1162.
[21] I.D. Rosca, F. Watari, M. Uo, T. Akasaka, Oxidation of multiwalled carbon nanotubes by nitric acid, Carbon 43 (15) (2005) 3124–3131.
[22] T. García-Mendiola, S. Requena-Sanz, E. Martínez-Periñán, I. Bravo, F. Pariente, E. Lorenzo, Influence of carbon nanodots on DNA-Thionine interaction. Application to breast cancer diagnosis, Electrochim. Acta 353 (2020) 136522.
[23] Y. Zeng, J. Bao, Y. Zhao, D. Huo, M. Chen, Y. Qi, M. Yang, H. Fa, C. Hou, A sandwich-type electrochemical immunoassay for ultrasensitive detection of non-small cell lung cancer biomarker CYFRA21-1, Bioelectrochemistry 120 (2018) 183–189.
[24] Y. Wang, J. Luo, J. Liu, X. Li, Z. Kong, H. Jin, X. Cai, Electrochemical integrated paper-based immunosensor modified with multi-walled carbon nanotubes nanocomposites for point-of-care testing of 17β-estradiol, Biosens. Bioelectron. 107 (2018) 47–53.
[25] G. Fusco, F. Gallo, C. Tortolini, P. Bollella, F. Ietto, A. De Mico, A. D'Annibale, R. Antiochia, G. Favero, F. Mazzei, AuNPs-functionalized PANABA-MWCNTs nanocomposite-based impedimetric immunosensor for 2,4-dichlorophenoxy acetic acid detection, Biosens. Bioelectron. 93 (2017) 52–56.
[26] M. Rizwan, S. Elma, S.A. Lim, M.U. Ahmed, AuNPs/CNOs/SWCNTs/chitosan-nanocomposite modified electrochemical sensor for the label-free detection of carcinoembryonic antigen, Biosens. Bioelectron. 107 (2018) 211–217.
[27] B. Lu, M.R. Smyth, R. O'Kennedy, Immunological activities of IgG antibody on pre-coated Fc receptor surfaces, Anal. Chim. Acta 331 (1) (1996) 97–102.
[28] J. Zhou, L. Du, L. Zou, Y. Zou, N. Hu, P. Wang, An ultrasensitive electrochemical immunosensor for carcinoembryonic antigen detection based on staphylococcal protein A—Au nanoparticle modified gold electrode, Sensor. Actuator. B Chem. 197 (2014) 220–227.
[29] M.H. Jazayeri, H. Amani, A.A. Pourfatollah, H. Pazoki-Toroudi, B. Sedighimoghaddam, Various methods of gold nanoparticles (GNPs) conjugation to antibodies, Sensing and Bio-Sensing Research 9 (2016) 17–22.
[30] Y. You, S. Lim, J. Hahn, Y.J. Choi, S. Gunasekaran, Bifunctional linker-based immunosensing for rapid and visible detection of bacteria in real matrices, Biosens. Bioelectron. 100 (2018) 389–395.
[31] K. Takemura, O. Adegoke, N. Takahashi, T. Kato, T.-C. Li, N. Kitamoto, T. Tanaka, T. Suzuki, E.Y. Park, Versatility of a localized surface plasmon resonance-based gold nanoparticle-alloyed quantum dot nanobiosensor for immunofluorescence detection of viruses, Biosens. Bioelectron. 89 (2017) 998–1005.
[32] S.-l. Hou, Z.-e. Ma, H. Meng, Y. Xu, Q.-h. He, Ultrasensitive and green electrochemical immunosensor for mycotoxin ochratoxin A based on phage displayed mimotope peptide, Talanta 194 (2019) 919–924.
[33] Y. Li, Y. Wang, L. Bai, H. Lv, W. Huang, S. Liu, S. Ding, M. Zhao, Ultrasensitive electrochemiluminescent immunosensing based on trimetallic Au-Pd-Pt/MoS2 nanosheet as coreaction accelerator and self-enhanced ABEI-centric complex, Anal. Chim. Acta 1125 (2020) 86–93.
[34] G.-C. Han, X. Su, J. Hou, A. Ferranco, X.-Z. Feng, R. Zeng, Z. Chen, H.-B. Kraatz, Disposable electrochemical sensors for hemoglobin detection based on ferrocenoyl cysteine conjugates modified electrode, Sensor. Actuator. B Chem. 282 (2019) 130–136.
[35] Z. Wang, Y. Chen, W. Dong, J. Zhou, B. Han, J. Jiao, L. Lan, P. Miao, Q. Chen, Copper (II)-ploy-L-histidine functionalized multi walled carbon nanotubes as efficient mimetic enzyme for sensitive electrochemical detection of salvianic acid A, Biosens. Bioelectron. 121 (2018) 257–264.
[36] J. Liu, L. Chen, H. Lu, Cardioprotective effect of salvianolic acid B against isoproterenol-induced inflammation and histological changes in a cardiotoxicity rat model, Trop. J. Pharmaceut. Res. 17 (11) (2018) 2189–2197.
[37] W. Xu, J. He, L. Gao, J. Zhang, C. Yu, Immunoassay for netrin 1 via a glassy carbon electrode modified with multi-walled carbon nanotubes, thionine and gold nanoparticles, Microchimica Acta 182 (13) (2015) 2115–2122.
[38] Y. Ding, Z. Chen, J. Xie, R. Guo, Comparative studies on adsorption behavior of thionine on gold nanoparticles with different sizes, J. Colloid Interface Sci. 327 (1) (2008) 243–250.
[39] Y. Liu, W. Wang, H. Wei, J. Li, X. Lu, X. Liu, Simultaneous determination of dihydroxybenzene isomers based on thionine functionalized multiwall carbon nanotubes modified electrode, J. Appl. Electrochem. 44 (5) (2014) 667–674.
[40] W. Lu, J. Ge, L. Tao, X. Cao, J. Dong, W. Qian, Large-scale synthesis of ultrathin Au-Pt nanowires assembled on thionine/graphene with high conductivity and sensitivity for electrochemical immunosensor, Electrochim. Acta 130 (2014) 335–343.
[41] C.-J. Gu, F.-Y. Kong, Z.-D. Chen, D.-H. Fan, H.-L. Fang, W. Wang, Reduced graphene oxide-Hemin-Au nanohybrids: facile one-pot synthesis and enhanced electrocatalytic activity towards the reduction of hydrogen peroxide, Biosens. Bioelectron. 78 (2016) 300–307.
[42] A.J. Bard, L.R. Faulkner, Electrochemical methods: fundamentals and applications, J. Chem. Educ. 60 (1980) first ed.
[43] D.S. Kim, Y.T. Kim, S.B. Hong, J. Kim, N.S. Heo, M.-K. Lee, S.J. Lee, B.I. Kim, I.S. Kim, Y.S. Huh, B.G. Choi, Development of lateral flow assay based on size-controlled gold nanoparticles for detection of hepatitis B surface antigen, Sensors 16 (12) (2016) 2154.
[44] B. Yin, W. Zheng, M. Dong, W. Yu, Y. Chen, S.W. Joo, X. Jiang, An enzyme-mediated competitive colorimetric sensor based on Au@Ag bimetallic nanoparticles for highly sensitive detection of disease biomarkers, Analyst 142 (16) (2017) 2954–2960.
[45] D.S. Kim, Y.T. Kim, S.B. Hong, J. Kim, N.S. Heo, M.-K. Lee, S.J. Lee, B.I. Kim, I.S. Kim, Y.S. Huh, B.G. Choi, Integration of organic electrochemical transistors and immuno-affinity membranes for label-free detection of interleukin-6 in the physiological concentration range through antibody–antigen recognition, Journal of Materials Chemistry B Materials for Biology & Medicine 6 (2018) 5400–5406.
[46] C. Russell, A.C. Ward, V. Vezza, P. Hoskisson, D. Alcorn, D.P. Steenson, D.K. Corrigan, Development of a needle shaped microelectrode for electrochemical detection of the sepsis biomarker interleukin-6 (IL-6) in real time, Biosens. Bioelectron. 126 (2019) 806–814.
[47] S.-b. Wang, S. Tian, F. Yang, H.-g. Yang, X.-y. Yang, G.-h. Du, Cardioprotective effect of salvianolic acid A on isoproterenol-induced myocardial infarction in rats, Eur. J. Pharmacol. 615 (1) (2009) 125–132.
[48] M.F. Nagoor Meeran, F. Laham, S. Azimullah, S. Tariq, S. Ojha, α-Bisabolol abrogates isoproterenol-induced myocardial infarction by inhibiting mitochondrial dysfunction and intrinsic pathway of apoptosis in rats, Mol. Cell. Biochem. 453 (1) (2019) 89–102.
[49] G. Rona, Catecholamine cardiotoxicity, J. Mol. Cell. Cardiol. 17 (4) (1985) 291–306.
[50] X. Han, P. Liu, M. Liu, Z. Wei, S. Fan, X. Wang, S. Sun, L. Chu, [6]-Gingerol Ameliorates ISO-Induced Myocardial Fibrosis by Reducing Oxidative Stress, Inflammation, and Apoptosis through Inhibition of TLR4/MAPKs/NF-Kb Pathway, Molecular Nutrition & Food Research (2020) 2000003, n/a(n/a).
[51] Q. Song, X. Chu, X. Zhang, Y. Bao, Y. Zhang, H. Guo, Y. Liu, H. Liu, J. Zhang, Y. Zhang, L. Chu, Mechanisms underlying the cardioprotective effect of Salvianic acid A against isoproterenol-induced myocardial ischemia injury in rats: possible involvement of L-type calcium channels and myocardial contractility, J. Ethnopharmacol. 189 (2016) 157–164.